Journal of Alloys and Compounds 498 (2010) 57–61

Contents lists available at ScienceDirect

Journal of Alloys and Compounds

journal homepage: www.elsevier.com/locate/jallcom

Structural and electrochemical characteristics of $Mg_{(55-x)}Ti_xNi_{(45-y)}Pt_y$ metal hydride electrodes

J.F.R. de Castro[a], S.F. Santos[b,*], F.R. Nikkuni[a], T.T. Ishikawa[c], E.A. Ticianelli[a]

[a] IQSC, Universidade de São Paulo, CP 780, CEP: 13560-970, São Carlos, SP, Brazil
[b] CECS, Universidade Federal do ABC, Rua Sta. Adélia 166, CEP: 09210-170, Bangu, Santo André, SP, Brazil
[c] DEMA, Universidade Federal de São Carlos, CP 676, CEP: 13560-905, São Carlos, SP, Brazil

ARTICLE INFO

Article history:
Received 23 October 2009
Received in revised form 9 March 2010
Accepted 9 March 2010
Available online 15 March 2010

Keywords:
Metal hydrides
Nanostructured materials
Mechanical alloying
Electrochemical reactions

ABSTRACT

In recent years, Mg–Ni-based metastable alloys have been attracting attention due to their large hydrogen sorption capacities, low weight, low cost, and high availability. Despite the large discharge capacity and high activity of these alloys, the accelerated degradation of the discharge capacity after only few cycles of charge and discharge is the main shortcoming against their commercial use in batteries. The addition of alloying elements showed to be an effective way of improving the electrode performance of Mg–Ni-based alloys. In the present work, the effect of Ti and Pt alloying elements on the structure and electrode performance of a binary Mg–Ni alloy was investigated. The XRD and HRTEM revealed that all the investigated alloy compositions had multi-phase nanostructures, with crystallite size in the range of 6 nm. Moreover, the investigated alloying elements demonstrated remarkable improvements of both maximum discharge capacity and cycling life. Simultaneous addition of Ti and Pd demonstrated a synergetic effect on the electrochemical properties of the alloy electrodes. Among the investigated alloys, the best electrochemical performance was obtained for the $Mg_{51}Ti_4Ni_{43}Pt_2$ composition (in at.%), which achieved 448 mAh g^{-1} of maximum discharge capacity and retained almost 66% of this capacity after 10 cycles. In contrast, the binary $Mg_{55}Ni_{45}$ alloy achieved only 248 mAh g^{-1} and retained 11% of this capacity after 10 cycles.

1. Introduction

The fast growing use of portable electronics in the last decade has been the main driving force behind the development of high energy density rechargeable batteries. Nickel-metal hydride (Ni-MH) batteries have 50% higher volumetric and gravimetric energy densities than the conventional Ni–Cd counterparts. Moreover, the absence of Cd in Ni-MH batteries is beneficial from the environmental point of view due to the high toxicity of this element [1–3].

Notwithstanding the abovementioned advantages of Ni-MH batteries, the continuous development in portable electronics, like color screens and longer operating times, demands battery cells with higher energy densities than the presently available [3]. The increase of energy density for Ni-MH batteries is closely related to the development of new negative electrode alloys with larger hydrogen storage capacities. Until now, only $LaNi_5$-based and Ti–Zr–V-based alloys have been used as anode materials in commercial Ni-MH cells. These alloys have low hydrogen storage capacities which limit the energy densities of the cells. Furthermore, their heavy weight and high costs are limiting factors as well [4]. Alternatives to these alloys are under investigation and magnesium–nickel alloys have been attracting much attention for this purpose due to their large hydrogen storage capacities, availability and relative low costs [3,4]. Conventional polycrystalline Mg–Ni alloys are not suitable to electrochemical hydrogen storage. Conversely, metastable Mg–Ni alloys (i.e., amorphous and nanocrystalline alloys) can be charged and discharged electrochemically and present high discharge capacities [5]. The synthesis of magnesium alloys by mechanical alloying demonstrated to be an effective way for obtaining alloy electrodes with high discharge capacities [5] but other non-conventional processing techniques like melt-spinning [6–9], hydriding combustion synthesis [10,11], thin film deposition [12–14], accumulative cold rolling [15], and so on, can be applied to this purpose.

The initial large discharge capacities displayed by metastable Mg–Ni alloys rapidly decay after few cycles of charge and discharge [3]. Such fast degradation has been attributed to the formation of magnesium hydroxide on the surface of alloy particles reducing the mass of active material and the charge transfer reaction kinetics in the electrolyte/active material interfaces [16]. Numerous investigations have been undertaken trying to overcome this

* Corresponding author. Tel.: +55 16 97737478.
E-mail address: Sydney.ferreira@ufabc.edu.br (S.F. Santos).

0925-8388/$ – see front matter © 2010 Elsevier B.V. All rights reserved.
doi:10.1016/j.jallcom.2010.03.097

problem. From the materials science point of view, these researches are focused on the modification of bulk and surface chemical compositions [3–9,12,14,17–19]. This last approach accomplished the best results for improving the electrochemical performances of the alloys until now.

Transition metals showed to be effective alloying elements for Mg–Ni alloys. These metal additions usually improve the electrode performance and have been intensively investigated. The replacement of Ti for Mg improved the cycling life performances of Mg–Ni alloy electrodes [20]. This behavior was attributed to the formation of TiO_2 on the alloy particle surfaces, retarding the oxidation of Mg. We reported improvements of cycling stabilities of alloy electrodes were also observed when 10 at.% of Co and Cr are added to a binary Mg–Ni alloy while increases of the maximum discharge capacity were achieved for the Zr, Cr and Nb additions [21]. The partial substitution of Zr for Mg in the ball-milled $Mg_{2-x}Zr_xNi$, with x ranging from 0 to 0.6, was reported by Zhang et al. [22]. These authors observed that the formation of an amorphous phase was favored when the amount of Zr increases in the alloys. They also reported that the maximum discharge capacity increases as a function of Zr content up to 0.4. Moreover, the cycling stability of the alloy electrodes is improved with the increase in Zr content. Partial substitution of Co for Ni also demonstrated a positive effect on the electrochemical properties of Mg_2Ni alloy synthesized by melt-spinning [7]. The maximum discharge capacity increased from 135.5 mAh g^{-1} (Co-free alloy) to 402.5 mAh g^{-1} for the $Mg_2(Ni_{0.6}Co_{0.4})$ alloy while the retained capacity after 20 cycles raised from 27.06 to 83.35%. The addition of Cu to the Mg_2Ni melt-spun alloy was investigated by Zhang et al. [9]. These authors observed that the addition of Cu increased the maximum discharge capacity of the ternary alloys up to certain Cu content while the electrode stability monotonously increased with the Cu content.

Multi-element Mg–Ni-based alloys were investigated by Anik et al. [23]. These authors investigated the ball-milled Mg–Ni–Ti–Zr alloys and observed a slight increase of the maximum discharge capacity for low Zr additions while for larger amounts of Zr the maximum discharge capacity drops. Both Zr and Ti are suitable to improve the cycling stability of the alloy electrodes. These authors also reported that further addition of Pd improved the electrochemical properties of the alloy while the addition of Co decreased these properties.

In addition to the transition metals, rare earths have been investigated as alloying elements to the Mg–Ni alloy electrodes. Huang et al. [8] investigated the effects of Nd addition on the electrode performance of the Mg–Ni binary alloy observing that the maximum discharge capacity increases for larger contents of Nd, reaching the highest values for Nd content in the range of 10–15 mol% (around 580 mAh g^{-1}). The retained capacity was 80% of the initial one after 20 cycles of charge/discharge. Ren et al. [24] investigated the addition of La to the Mg_2Ni melt-spun alloy. The structural characterization of La-free and La-containing alloys showed that the first ones are fully crystalline while the latter ones have larger fractions of amorphous phase indication an increase of the glass forming ability promoted by La addition. These authors also observed that the increase of La content resulted in remarkable raise of the maximum discharge capacity. Moreover, the cycling stability of the alloys containing larger amounts of La into their compositions was improved.

Noble metals also have been investigated as alloying elements for Mg–Ni alloy electrodes. The most investigated alloy system of this type is Mg–Ni–Pd which usually displays improvements of cycling durability as costs of the maximum discharge capacities [25–27]. Similar behavior was reported by Tian et al. [28] for the Mg–Ni–Ti–Pd alloys. The improved cycling stability observed in this alloy system was ascribed to the formation of a multi-oxide passive layer composed by a number of Pd and Ti oxides which could reduce the oxidation of Mg [29].

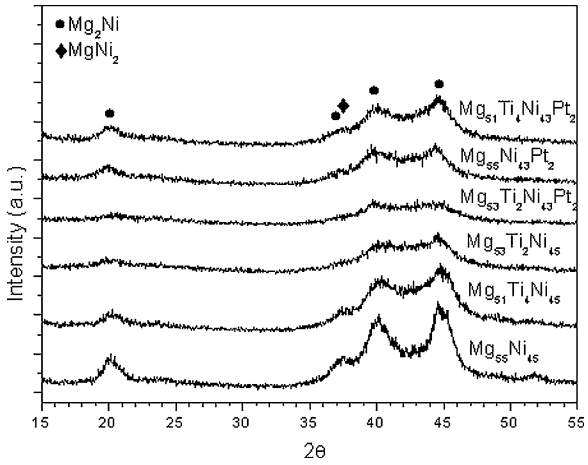

Fig. 1. XRD patterns of the $Mg_{(55-x)}Ti_xNi_{(45-y)}Pt_y$ alloys.

The addition of Pt to Mg–Ni alloy electrodes was reported by the first time by Souza et al. [30]. These authors observed that the addition of only 2 at.% of Pt was enough to increase the maximum discharge capacity and improve the cycling performance of the alloy electrode.

In the present work Mg–Ni–Ti–Pt quaternary alloys were investigated by the first time as anode materials for Ni-MH batteries. This investigation was motivated by the possibility of improving the good electrochemical properties reported for the Mg–Ni–Ti and Mg–Ni–Pt alloys. The synthesized alloys had their structures and electrochemical properties evaluated by means of X-ray diffraction (XRD), high-resolution transmission electron microscopy (HRTEM) and galvanostatic charge and discharge cycles.

2. Experimental

The investigated quaternary alloys have general compositions of $Mg_{(55-x)}Ti_xNi_{(45-y)}Pt_y$, where $0 \le x \le 4$ and $y = 0$ and 2 (all quantities in at.%). The alloys were synthesized by mechanical alloying; starting from Ni and Pt powders and Mg granulates with 99.7, 99.9 and 98% of purity, respectively. The millings were performed using a Spex 8000 shaker mill. The ball to powder weigh ratio was 10:1 and the milling time was 6 h. The samples were handled in a glove-box under argon to minimize oxidation.

The microstructures of the investigated alloys were analyzed by high-resolution transmission electron microscopy (HRTEM) and X-ray diffraction (XRD) using a JEOL JEM – 3010 ARP microscope, operating at 300 kV, and a Siemens D5005 diffractometer, with Cu-Kα radiation, respectively. TEM image treatment was performed using a Gatan Digital – Micrograph package.

The alloy electrodes were prepared by cold pressing a mixture of 0.1 g active material (alloy powder) and 0.1 g blend of carbon black (Vulkan XC-72R) with 33 wt.% of polytetrafluoroethylene (PTFE) binder in both sides of a 2 cm^2 nickel screen. The electrochemical tests were carried out in a three electrode cell configuration, with a Pt counter electrode, an Hg/HgO reference electrode and a 6 mol/L KOH electrolyte. The charge and discharge current densities of the electrodes were 200 mA g^{-1} and 20 mA g^{-1} of active material, respectively. The cut-off potential was −0.65 V (*vs.* Hg/HgO, KOH 6 mol/L).

3. Results and discussion

3.1. Structural characteristics

Fig. 1 shows the XRD patterns of the investigated alloys, where it is possible to observe some broadened diffraction peaks superimposing a wide band localized in the range of 35–47°. These features may be related to the co-existence of nanocrystalline and amorphous phases in these alloys. In the binary Mg–Ni alloy, the nanocrystalline phases observed in the patterns were identified as: Mg_2Ni and $MgNi_2$. In the other alloys, the Mg_2Ni peaks are still visible, even though they are quite broadened in the $Mg_{53}Ti_2Ni_{45}$ and $Mg_{53}Ti_2Ni_{43}Pt_2$ alloys. Conversely, the $MgNi_2$ phase is hardly

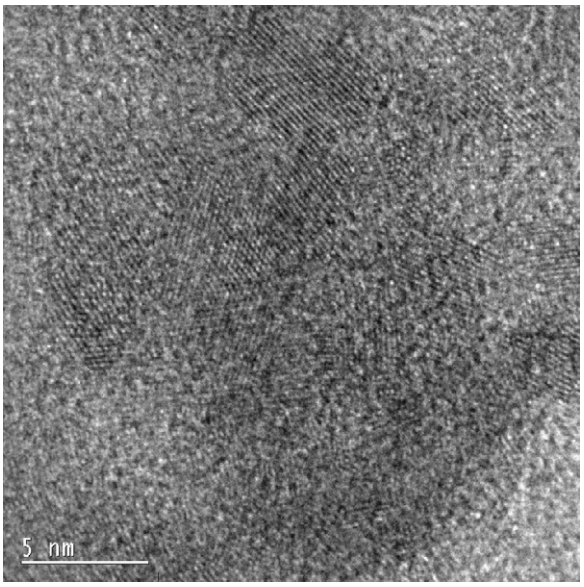

Fig. 2. HRTEM image (bright field) of the $Mg_{55}Ni_{45}$ alloy.

observed in the $Mg_{51}T_4Ni_{45}$ and $Mg_{51}Ti_4Ni_{43}Pt_2$ alloys and it is not distinguishable in the $Mg_{55}Ni_{43}Pt_2$, $Mg_{53}Ti_2Ni_{43}Pt_2$, and $Mg_{53}Ti_2Ni_{45}$ alloys.

The bright field HRTEM images of the $Mg_{55}Ni_{45}$ and $Mg_{51}Ti_4Ni_{43}Pt_2$ alloys are shown in Figs. 2 and 3, respectively. In both alloys the co-existence of nanocrystalline and amorphous phases can be noted by the presence of nanocrystalline grains and some disordered (amorphous) regions. Observing a number of HRTEM images of these alloys, the average crystallite size was estimated to be around 6 nm for all samples.

3.2. Electrochemical characteristics

Fig. 4 shows the discharge capacity *vs*. cycling number curves for the investigated binary and ternary alloys. All alloys presented the maximum discharge capacity at the first cycle, indicating high initial electrochemical activity, which is the typical behavior of ball-milled Mg–Ni alloys [3–5]. The improvement of the electrode performance observed for the ternary alloys is noticeable when compared to the original binary one. Additions of Ti or Pt lead to an increase of both the maximum discharge capacity and the cycling stability. The most prominent result was achieved by the $Mg_{55}Ni_{43}Pt_2$, which reached a maximum discharge capacity of 425 mAh g^{-1} while for the $Mg_{55}Ni_{45}$ alloy the capacity was 247 mAh g^{-1}.

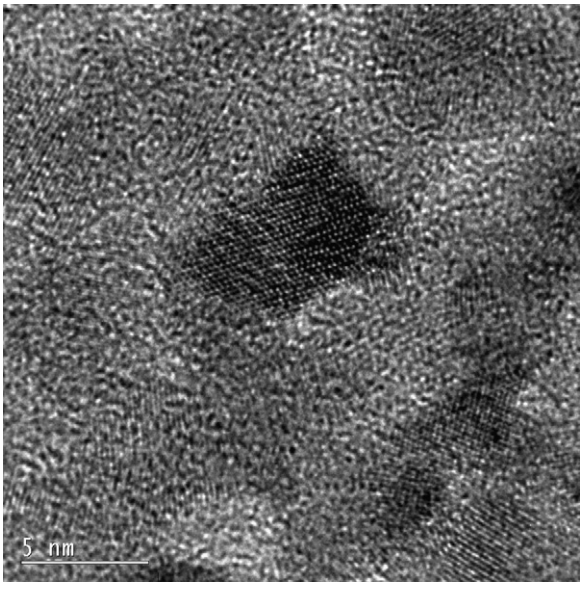

Fig. 3. HRTEM image (bright field) of the $Mg_{51}Ti_4Ni_{43}Pt_2$ alloy.

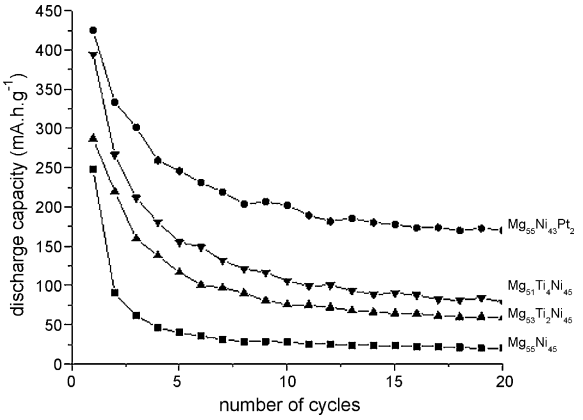

Fig. 4. Curves of discharge capacity *vs*. number of cycles for the investigated binary and ternary alloys.

Table 1 illustrates the quantitative results concerning the electrochemical performance of the binary and ternary alloy electrodes. The cyclic performance of the electrodes was evaluated by the retained capacity at the *n*th cycle (k_n) and the average retained capacity (k_{ave}), which in the present work is defined as:

$$k_n = \frac{C_n}{C_{\max}} \quad (1)$$

where C_n is the discharge capacity at the *n*th of charge/discharge cycle and $C_{\max}$ is the maximum discharge capacity of the electrode, and

$$k_{ave} = \frac{k_5 + k_{10} + k_{20}}{3} \quad (2)$$

As shown in Table 1, both alloying elements (Ti and Pt) were effective to decrease the degradation rate of the electrodes when compared to the Mg–Ni binary alloy. In the case of Ti substitution for Mg, there was no enhancement on the cyclic stability when the amount of alloying element increased from 2 to 4 at.% of Ti, although the maximum discharge capacity of the latter raised from 287.2 mAh g^{-1} to 394.6 mAh g^{-1}. Replacement of Pt for Ni increased both the cycling stability and the maximum discharge capacity of the electrode. Comparing the alloy with 2 at.% of Pt with that one with the same amount of Ti, it is possible to observe that Pt addition is remarkably more effective to improve the electrochemical properties of the Mg–Ni alloy. The maximum discharge capacity and the cycling stability of the Pt alloy are, respectively, about 50 and 40% superior when compared to the alloy with 2% Ti. Even the alloy with 4% of Ti has inferior electrode performance than the alloy with 2% Pt, especially in terms of cyclic stability.

Souza et al. [30] investigated the simultaneous substitution of Pt for Ni and Mg in the $Mg_{50}Ni_{50}$ alloy. The general composition

Table 1
Parameters of electrochemical performance for the binary and ternary alloys.

Alloy	$C_{\max}$ (mAh g^{-1})	k_5 (%)	k_{10} (%)	k_{20} (%)	k_{ave} (%)
$Mg_{55}Ni_{45}$	247.7	16.1	11.2	8.0	11.8
$Mg_{53}Ti_2Ni_{45}$	287.2	40.6	26.3	20.4	29.1
$Mg_{51}Ti_4Ni_{45}$	394.6	39.3	26.9	19.9	28.7
$Mg_{55}Ni_{43}Pt_2$	425.2	57.8	47.6	40.1	48.5

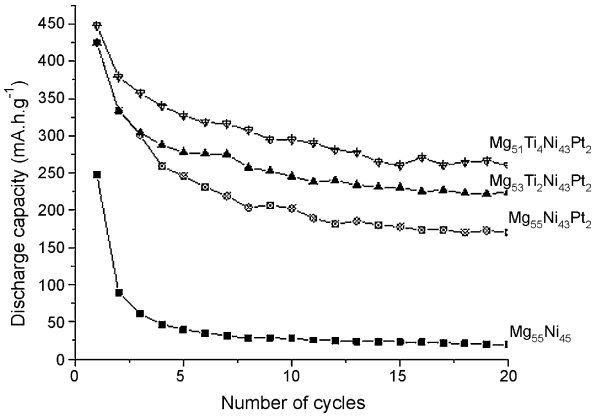

Fig. 5. Electrochemical performance of $Mg_{55}Ni_{45}$ and the Pt-containing alloys.

of ternary alloys was $Mg_{(50-x/2)}Ni_{(50-x/2)}Pt_x$ and the best results were obtained for the $Mg_{49}Ni_{49}Pt_2$ alloy, which presented a maximum discharge capacity of 380 mAh g^{-1} and retained capacity of 33% of its initial capacity after 10th cycles. This value is lower than that obtained for the $Mg_{55}Ni_{43}Pt_2$ alloy presented in this work (see Table 1).

In the case of the Mg–Ni–Ti system, there is some dispersion in the values of electrode performances reported in the literature. These discrepancies arise from the differences in: the alloy compositions, microstructure of the end products (fully amorphous, fully nanocrystalline, mixtures of amorphous and nanocrystalline phases, and so forth), and electrochemical test conditions (different current densities of charge and discharge, different cut-off potentials, and so on) [20,31]. So far we have noticed that the largest discharge capacity obtained in the Mg–Ni–Ti system was 575 mAh g^{-1} for the $MgNi_{0.95}Ti_{0.05}$ multi-phase alloy [20] but, on the other hand, the increase of the maximum discharge capacity due to the addition of Ti was not so high in this report, rising from 522 mAh g^{-1} (39% of retained capacity after 10th cycles) to 575 mAh g^{-1} (46% of retained capacity after 10th cycles), for the Mg–Ni and $MgNi_{0.95}Ti_{0.05}$ alloys, respectively. The better performance obtained for the Mg–Ni binary alloy in Ref. [20] compared to the results of the present work can be credited to different chemical compositions and mainly to different microstructures of the alloys, i.e., a mixture of amorphous and nanocrystalline phases in the present work and fully amorphous alloy in Ref. [20].

Fig. 5 shows the discharge capacity curves for the binary $Mg_{55}Ni_{45}$ and the Pt-containing alloys. The maximum discharge capacity was nearly the same for the $Mg_{55}Ni_{43}Pt_2$ and the $Mg_{53}Ti_2Ni_{43}Pt_2$ alloys and slightly higher for the $Mg_{41}Ti_4Ni_{43}Pt_2$ alloy. Comparing the curves for the $Mg_{55}Ni_{43}Pt_2$ and the $Mg_{53}Ti_2Ni_{43}Pt_2$ electrodes (Fig. 5), it is noticeable that the addition of Ti resulted in further enhancement of cycling stability of the electrode, for the same maximum discharge capacity. When the amount of Ti increases from 2 to 4%, the maximum discharge capacity rises from 424.5 mAh g^{-1} to 448 mAh g^{-1}.

Table 2 presents the maximum discharge capacities and cycling life parameters of the $Mg_{55}Ni_{45}$ and the Pt-containing alloys. The values of k_{ave} greatly increased with the addition of 2 at.% of Pt, reaching 48.5%, which is over 4 times the value obtained for the binary alloy. The stability of the alloy electrodes, Table 2, continuously increases with the additions of Ti. Comparing the results of the alloys containing 2 and 4% of Ti, with and without Pt, the different behavior caused by the addition of Pt is noticeable. When the amount of Ti increased from 2 to 4% in the Pt-free alloys, the cycling stability was not improved (Table 1). Conversely, for the Pt-containing alloys, the increase of the amount of Ti promoted further enhancement of cycling stability (Table 2).

Table 2
Electrochemical performance of the binary and Pt-containing alloys.

Alloy	C_{max} (mAh g^{-1})	k_5 (%)	k_{10} (%)	k_{20} (%)	k_{ave} (%)
$Mg_{55}Ni_{45}$	247.7	16.1	11.2	8	11.8
$Mg_{55}Ni_{43}Pt_2$	425.15	57.8	47.6	40.1	48.5
$Mg_{53}Ti_2Ni_{43}Pt_2$	424.5	65.5	57.8	52.8	58.7
$Mg_{51}Ti_4Ni_{43}Pt_2$	448	73	65.8	58	65.8

3.3. Effects of Ti and Pt additions on the electrode performances

Previous studies about the degradation of Mg–Ni alloy electrodes indicated that the decay of discharge capacity is associated to the low stability of these alloys in alkaline media which leads to the formation of $Mg(OH)_2$ on the particle surfaces [16]. The formation of this passive film reduces the charge transfer reaction kinetics at the electrolyte/particle interfaces. Moreover, the formation of $Mg(OH)_2$ resulted in mass loss of active material of the electrode. In the case of Mg–Ni–Ti alloys, slower degradation kinetics of the discharge capacities when compared to the Ti-free alloys is observed. This behavior was attributed to a preferential oxidation of Ti on the surface of these alloys [20,31]. Thus, the formation of a TiO_2 passive thin film on the alloy particles would retard the formation of magnesium hydroxide [20,31].

Actually, the problems related to the poor corrosion resistance of Mg and its alloys are not new and have been a limiting factor for several applications [32]. The limited solubility and in some cases the complete immiscibility between Mg and several transition metals has motivated the development of Mg metastable alloys with extended solubility, aiming to obtain new alloy compositions with improved corrosion resistances. In the case of Mg–Ti system, the mutual solubility of Mg and Ti in any phase is quite low, and no intermetallic compounds occur in this system. Thus, to effectively promote the alloying between Mg and Ti, non-conventional methods of synthesis have been employed, such as physical vapor deposition (PVD) [33,34]. The application of these non-conventional synthesis methods for the Mg–Ti system produced extended Mg(Ti) solid solutions with amounts of Ti reaching up to 46 at.% [33]. Corrosion studies of the Mg–44% Ti alloy thin films showed remarkable increase of the corrosion resistance when compared to pure Mg. The explanation offered by the authors to this enhancement of corrosion resistance was that probably Ti formed a protective surface film which acted in a similar way of Cr in Fe–Cr system, into which a network of metal–oxygen–metal linkages is formed on the alloy surface thereby suppressing the dissolution of the more active underling Mg-rich matrix [33]. Baliga et al. [35] investigate the surface film formed on Mg(Ti) solid solutions synthesized by PVD technique and their results suggest the formation of TiO_2 on the surface of the alloys during processing. The presence of this phase should be closely related to the high corrosion resistance of these alloys because TiO_2 is insoluble in aqueous solution and stable in a wide range of pH [35]. In a latter investigation, Baliga and Tsakiropoulos [36] suggested that the corrosion resistance could be ascribed to the formation of Ti spinels during corrosion. In the case of fully amorphous Mg–Ni–Ti alloy electrodes synthesized by mechanical alloying, the presence of titanium oxide was also suggested by XPS results in alloys after repeated cycles of charge and discharge. It has also been noted that in Mg–Ni alloys with additions of Ti, the oxidation of Mg was prevented in some extent [31]. On the other hand, the Ti-containing alloys synthesized by mechanical alloying probably do not have the same corrosion resistance of thin films with the same chemical compositions since the last ones are probably more chemically homogeneous. The degree of chemical homogeneity strongly affects the corrosion resistance of Mg–Ti alloys. There are results indicating that heterogeneous distribution of Ti, resulting in different concentrations of this element along the

microstructure, could favor localized corrosion due to formation of micro-galvanic pairs between Ti reach and Ti poor regions [34].

Until now, there are few published works dealing the effect of noble metal additions to Mg–Ni–Ti alloy [28,29,37]. Tian et al. [37] investigated the Mg–Ti–Pd–Ni system. These authors synthesized fully amorphous $Mg_{0.9-x}Ti_{0.1}Pd_xNi$ alloys, with x ranging from 0.04 to 0.1, by mechanical alloying and observed improvements of cycling stability with addition of Pd to the ternary $Mg_{0.9}Ti_{0.1}Ni$ alloy. These results were justified by the formation of dense and stable passive films on the particle surfaces, preventing the Mg oxidation. XPS and AES results indicated a decrease of Mg oxidation when the amount of Pd increases. The authors related the presence of NiO, PdO, and TiO_2 phases on the surfaces of the particles and ascribed the reduction of Mg oxidation to the formation of a complex passive film composed by the mixture of these three oxides. Moreover, the addition of Pt to the Mg alloy should displace the corrosion potential of the alloys reinforcing their cathodic character in a similar way of that observed for the Ti–Pd and Ti–Pt alloys [38,39].

Taking these previous works in consideration, it is expectable to have an increase of cycling performance for the investigated Ti-containing alloy electrodes due to the passive film formation promoted by Ti. This behavior is in fact observed by the larger values of k_{ave} for the Mg–Ni–Ti alloys when compared to that one observed for the Mg–Ni binary alloy (Table 1).

In the case of the quaternary alloys investigated in this work, the same mechanism of degradation protection depicted by Tian et al. [37] for the Mg–Ni–Ti–Pd alloys is expected to take place for the presently studied Mg–Ni–Ti–Pt ones. Moreover, the addition of Pt should reinforce the cathodic behavior of these alloys thus increasing their stabilities in alkaline solution. The presented results also allowed observing a synergetic behavior of corrosion protection when both Pt and Ti are added to the Mg–Ni alloy. When the amount of Ti is increased in the quaternary alloys, the durability of the alloy electrode is increased too. This behavior is not observed for the Pt-free ternary alloys where the increase of Ti content did not exerted any influence on the electrode durability (Tables 1 and 2).

In this work there is no direct assessment to the structure and chemical composition of the passive film formed on the alloy electrode surfaces. The lack of surface analysis is justified by the fact that the alloys investigated in this work are multi-phase. Thus, surface investigation by XPS profiling becomes more complex and less reliable. The reason of that arises from the influence of several issues such as phase morphologies, preferential latching of phases, partitioning of chemical elements between different phases, different surface geometries depending on the present phases, and sputtering rate of each one of these phases, which drastically affect the data analysis of XPS results [40].

4. Conclusions

The Mg–Ni–Ti and Mg–Ni–Pt ternary alloys investigated in the present work showed an increase of the maximum discharge capacity and better cycling stability than the binary $Mg_{55}Ni_{45}$ alloy electrode. The addition of Pt showed to be more effective than Ti for improving the electrochemical properties of the alloy electrodes. The simultaneous addition of Ti and Pt showed even better electrochemical performance of the alloy electrodes than the ternary alloys. For the Mg–Ni–Ti–Pt alloys, it was observed that the increase of Ti content causes an improvement of the cycling stability of the alloy electrodes. This behavior was not observed for the Pt-free alloys. The better cycling stability of the Mg–Ni–Ti–Pt alloys can be ascribed to the formation of dense multi-phase passive film layers on the particle surfaces and also to the displacement of corrosion potential to more cathodic values, slowing down the degradation rate of the alloy electrodes. The best electrochemical properties were obtained for the $Mg_{51}Ti_4Ni_{43}Pt_2$ alloy which exhibited a maximum discharge capacity of 448 mAh g^{-1} and retained 65.8% of its initial discharge capacity after 10 cycles.

Acknowledgements

The authors gratefully acknowledge the financial support of São Paulo State Science Foundation (FAPESP) and the Brazilian National Research Council (CNPq). The authors also acknowledge to the Electron Microscopy Laboratory of LNLS – Campinas – Brazil for the utilization of the high-resolution transmission electron microscope.

References

[1] M.A. Fetcenko, S.R. Ovshinsky, B. Reichman, K. Young, C. Fierro, A. Zallen, W. Mays, T. Ouchi, J. Power Sources 165 (2007) 544–551.
[2] P.H.L. Notten, M. Ouwerkerk, H. van Hal, D. Beelen, W. Keur, J. Zhuo, H. Feil, J. Power Sources 129 (2004) 45–54.
[3] S.F. Santos, T.T. Ishikawa, E.A. Ticianelli, in: J.R. Telle, N.A. Pearstine (Eds.), Amorphous Materials: Research, Technology and Applications, Nova Science Publishers, 2009, pp. 219–237.
[4] X. Zhao, L. Ma, Int. J. Hydrogen Energy 34 (2009) 4788–4796.
[5] M. Anik, J. Alloys Compd. 491 (2010) 565–570.
[6] S. Kalinichenka, L. Rontzsch, Kieback, Int. J. Hydrogen Energy 34 (2009) 7749–7755.
[7] Y.-H. Zhang, H.-P. Ren, B.-W. Li, S.-H. Guo, Z.-G. Pang, X.-L. Wang, Int. J. Hydrogen Energy 34 (2009) 8144–8151.
[8] L.-J. Huang, J.-G. Tang, Y. Wang, J.-X. Liu, D.C. Wu, J. Alloys Compd. 485 (2009) 186–191.
[9] Y.-H. Zhang, D.-L. Zhao, B.-W. Li, H.-P. Ren, S.-H. Guo, X.-L. Wang, J. Alloys Compd. 491 (2010) 589–594.
[10] X.F. Liu, Y.F. Zhu, L.Q. Li, J. Alloys Compd. 425 (2006) 235–238.
[11] Y. Zhu, Y. Wang, L. Li, Int. J. Hydrogen Energy 33 (2008) 2965–2969.
[12] P. Vermeulen, P.C.J. Graat, H.J. Wondergem, P.H.L. Notten, Int. J. Hydrogen Energy 33 (2008) 5646–5650.
[13] S. Bouhtiyya, L. Roué, Int. J. Hydrogen Energy 34 (2009) 5778–5784.
[14] J. Xu, Y. Li, F. Wang, Electrochim. Acta 55 (2009) 148–154.
[15] S. Pedneault, J. Huot, L. Roué, J. Power Sources 185 (2008) 566–569.
[16] W. Liu, Y. Lei, D. Sun, J. Wu, Q. Wang, J. Power Sources 58 (1996) 243–247.
[17] S.F. Santos, J.F.R. de Castro, T.T. Ishikawa, E.A. Ticianelli, J. Mater. Sci. 43 (2008) 2889–2894.
[18] B. Khorkounov, A. Gebert, Ch. Mikel, L. Schultz, J. Alloys Compd. 458 (2008) 479–486.
[19] E.C. Souza, E.A. Ticianelli, Int. J. Hydrogen Energy 32 (2007) 4917–4924.
[20] S. Ruggeri, L. Roué, J. Huot, R. Schulz, L. Aymard, J.-M. Tarascon, J. Power Sources 112 (2002) 547–556.
[21] S.F. Santos, J.F.R. de Castro, T.T. Ishikawa, E.A. Ticianelli, J. Alloys Compd. 434–435 (2007) 756–759.
[22] Y.-H. Zhang, X.-Y. Han, B.-W. Li, H.-P. Ren, X.-P. Dong, X.-L. Wang, J. Alloys Compd. 450 (2008) 208–214.
[23] M. Anik, I. Akay, G. Ozdemir, B. Baksan, Int. J. Hydrogen Energy 34 (2009) 9765–9772.
[24] H.-P. Ren, Y.-H. Zhang, B.-W. Li, D.-L. Zhao, S.-H. Guo, X.-L. Wang, Int. J. Hydrogen Energy 34 (2009) 1429–1436.
[25] S.-I. Yamaura, H.-Y. Kim, H. Kimura, A. Inoue, Y. Arata, J. Alloys Compd. 347 (2002) 239–243.
[26] T. Ma, Y. Hatano, T. Abe, K. Watanabe, J. Alloys Compd. 372 (2004) 251–258.
[27] J.F.R. de Castro, S.F. Santos, T.T. Ishikawa, E.A. Ticianelli, Proceedings of the Brazilian MRS Meeting, Natal, RN, Brazil, 2008.
[28] Q.-F. Tian, Y. Zhang, H.-L. Chu, L.-X. Sun, F. Xu, Z.-C. Tan, H.-T. Yuan, T. Zhang, J. Power Sources 159 (2006) 155–158.
[29] Q. Tian, Y. Zhang, Y. Wu, J. Alloys Compd. 484 (2009) 763–771.
[30] E.C. Souza, J.F.R. de Castro, E.A. Ticianelli, J. Power Sources 160 (2006) 1425–1430.
[31] S.-C. Han, P.S. Lee, J.-Y. Lee, A. Zuttel, L. Schlapbach, J. Alloys Compd. 306 (2000) 219–226.
[32] C.M.A. Brett, L. Dias, B. Trindade, R. Fischer, S. Mies, Electrochim. Acta 51 (2006) 1752–1760.
[33] K.R. Baldwin, D.J. Bray, D.G. Howard, R.W. Gardiner, Mater. Sci. Technol. 12 (1996) 937–943.
[34] T. Mitchell, S. Diplas, P. Tsakiropoulos, J. Alloys Compd. 392 (2005) 127–141.
[35] C.B. Baliga, P. Tsakiropoulos, S.B. Dodd, R.W. Gardiner, in: G.W. Lorimer (Ed.), Proceedings of the Third International Mg Conference, Institute of Materials, London, 1997, p. 627.
[36] C.B. Baliga, P. Tsakiropoulos, Mater. Sci. Eng. A 134 (1991) 1029–1032.
[37] Q.-F. Tian, Y. Zhang, L.-X. Sun, F. Xu, Z.-C. Tan, H.-T. Yuan, T. Zhang, J. Power Sources 158 (2006) 1463–1471.
[38] M. Nakagawa, S. Matsuya, K. Udoh, Dental Mater. J. 20 (2001) 305–314.
[39] M. Nakagawa, S. Matsuya, K. Udoh, Dental Mater. J. 21 (2002) 83–92.
[40] K.J. Gross, D. Chartouni, E. Leroy, A. Zuttel, L. Schlapbach, J. Alloys Compd. 269 (1998) 259–270.